# Cramér–Rao Bound Analysis on Multiple Scattering in Multistatic Point-Scatterer Estimation

Gang Shi, *Student Member, IEEE*, and Arye Nehorai, *Fellow, IEEE*

***Abstract*—The resolution improvements of time reversal methods through exploiting nonhomogeneous media have attracted much interest recently with broad applications, including underwater acoustics, radar, detection of defects in metals, communications, and destruction of kidney stones. In this paper, we analyze the effect of inhomogeneity generated by multiple scattering among point scatterers under a multistatic sensing setup. We derive the Cramér–Rao bounds (CRBs) on parameters of the scatterers and compare the CRBs for multiple scattering using the Foldy–Lax model with the reference case without multiple scattering using the Born approximation. We find that multiple scattering could significantly improve the estimation performance of the system and higher order scattering components actually contain much richer information about the scatterers. For the case where multiple scattering is not possible, e.g., where only a single target scatterer exists in the illuminated scenario, we propose the use of *artificial scatterers*, which could effectively improve the estimation performance of the target despite a decrease in the degrees of freedom of the estimation problem due to the introduced unknown parameters of the artificial scatterers. Numerical examples demonstrate the advantages of the artificial scatterers.**

***Index Terms*—Artificial scatterer, born approximation, Cramér–Rao bound (CRB), Foldy–Lax model, inhomogeneity, multiple scattering, multistatic.**

## I. Introduction

THE TIME reversal approach [1] and its super resolution [2] have attracted increasing interest recently with broad applications, including underwater acoustics, radar, detection of defects in metals, communications, and destruction of kidney stones. The idea behind so-called *physical time reversal* is to record a signal emitted by sources or reflected by targets using an array of transducers and then transmit the time-reversed and complex conjugated version of the measurements back into the medium. In a reciprocal medium, the back-propagated wave will then retrace the original trajectory and focus around the original source locations. If the medium is homogeneous, the diffraction resolution of the refocused field in the direction parallel to a linear array (or cross-range resolution) is $\lambda R/a$, and $\lambda(R/a)^2$ in the perpendicular direction (or range resolution) [3], [4], where $\lambda$ is the carrier wavelength, $R$ is the range between the array and the source, and $a$ is the array aperture. Experimental and theoretical evidence [5], [6] shows that refocusing in a nonhomogeneous or random medium is much tighter than in homogeneous, which is referred to as the *super-resolution* of the time reversals [2]. This super-resolution is intuitively interpreted as taking advantage of the inhomogeneity to distribute the wave over a larger part of the medium and, therefore, carry more information about the source [2], and it is quantitatively measured as the improved *effective aperture* [2], which corresponds to the equivalent aperture that produces the same refocusing resolution in a reference homogeneous medium.

Encouraged by results in the situation of inhomogeneity, we investigate possible advantages of multiple scattering in the case of point-scattering estimation, in which the inhomogeneity is induced by interactions among the scatterers. Multiple scattering exists in many physical systems involving wave propagation, including electrons, ultrasound, electromagnetic, and seismic waves, and can be analyzed using very much the same approaches, as explained in [7]. Though modeling and understanding of multiple scattering has been of interest in various domains ranging from solid-state physics to optics to seismology [8], it is still widely ignored in the signal processing literature [9]–[16], to the best of the authors' knowledge. In [7], [8], and [17]–[21], the effect of multiple scattering on the refocusing of the time reversal is studied experimentally and analytically, and experiments conducted in [22] demonstrate that multiple scattering can help by increasing the information transfer rate in ultrasonic communications. Recently, MUSIC and maximum likelihood (ML) algorithms for estimating the locations of point scatterers with multiple scattering were proposed in [23]–[26]. Cramér–Rao bounds (CRBs) are computed in [27] and [28] to evaluate the performance of reflectivity estimation in an unknown environment using physical time reversal ignoring multiple scattering. In this paper, we continue our work in [25] and [26] by evaluating the effect of multiple scattering on the performance of point-scatterer estimation. We will evaluate multiple scattering under an active multistatic sensing setup without physical time reversals, and measure the estimation performance in terms of the well-known CRB benchmark. We find that multiple scattering could significantly improve the estimation performance of the system in most of randomized system setups. We will also propose the use of *artificial scatterers* to create multiple scattering for the case where it is not available. Interestingly, we find that the artificial scatterers could effectively improve the estimation performance

Manuscript received December 8, 2005; revised September 19, 2006. The associate editor coordinating the review of this manuscript and approving it for publication was Dr. Jean Pierre Delmas. This work was supported in part by the DARPA/AFOSR under Grant FA9550-04-1-0187 and by AFOSR under Grant FA9550-05-1-0018. This work was presented in part at the IEEE ICASSP'2006.

G. Shi was with the Department of Electrical and Systems Engineering, Washington University in St. Louis, St. Louis, MO 63130 USA. He is now with the Division of Biostatistics, Washington University School of Medicine, St. Louis, MO 63130 USA (e-mail: gang@wubios.wustl.edu).

A. Nehorai is with the Department of Electrical and Systems Engineering, Washington University in St. Louis, St. Louis, MO 63130 USA (e-mail: nehorai@ese.wustl.edu).

Digital Object Identifier 10.1109/TSP.2007.893956

of the target despite a decrease in the degrees of freedom due to the introduced unknown parameters.

This paper is organized as follows. In Section II, we present two physical models used in later comparisons: one takes into account the multiple scattering among the scatterers using the Foldy–Lax model [29]–[32], and the other ignores it by using the Born approximation [29], [33]. In Section III, we compute the CRBs based on these two physical models and then present numerical comparisons of the CRBs under randomized setups in Section IV. In Section V, we propose the use of artificial scatterers to improve the system performance and present conclusions in Section VI.

## II. Models and Problem Statement

We review two physical models of the multistatic response matrix [3], [34], [35]: one includes multiple scattering using the Foldy–Lax model and the other assumes single reflection using the Born approximation. For more details, readers are referred to [23]–[26].

We consider a transmit array of $N_t$ isotropic point antennas centered at known positions $\boldsymbol{\alpha}_1, \boldsymbol{\alpha}_2, \ldots, \boldsymbol{\alpha}_{N_t}$, and a receive array of $N_r$ sensors at $\boldsymbol{\beta}_1, \boldsymbol{\beta}_2, \ldots, \boldsymbol{\beta}_{N_r}$. The so-called **multistatic response matrix** [3], [34], [35] $K = [K_{j,k}(\omega)]$, represented in frequency domain, is of dimension $N_r \times N_t$, whose element $K_{j,k}(\omega)$ coincides with the received signal at the $j$th receive antenna due to an impulse excitation (in the frequency domain) at a frequency $\omega$ applied by the $k$th transmit antenna [35], where $j = 1, 2, \ldots, N_r$ and $k = 1, 2, \ldots, N_t$. We assume the scenario under probe is stationary during the period of sensing. For ease of understanding, the multistatic matrix could be interpreted as the counterpart to a channel matrix in a multiple-input multiple-output (MIMO) wireless communication system. However, since in sensing problems it is of more interest to extract the information about the probed scenario than to transmit information from the transmit array to the receive array, we assume that there is no direct link from any transmit antenna to the receive antennas, i.e., the measured fields at the receive array are due solely to the scattering of the illuminated scenario. Note that since the information about the scenario is fully embedded in the multistatic matrix, the inference on the probed scenario will be based on the measured multistatic matrix in this paper, which could be obtained by sending signal at the transmit antennas once a time or employing a set of linearly independent signal simultaneously at different transmit antennas.

We consider a scenario as illustrated in Fig. 1 that consists of $M$ discrete point scatterers in a known background medium. The locations and scattering potentials of the scatterers are assumed unknown, denoted by $\boldsymbol{x}_1, \boldsymbol{x}_2, \ldots, \boldsymbol{x}_M$ and $\tau_1(\omega), \tau_2(\omega), \ldots, \tau_M(\omega)$, respectively. The time harmonic Green's function $G(\boldsymbol{r}, \boldsymbol{r}', \omega)$ of the background, which represents the "propagator" from a location $\boldsymbol{r}'$ to $\boldsymbol{r}$ at frequency $\omega$, satisfies the reduced wave equation [3]

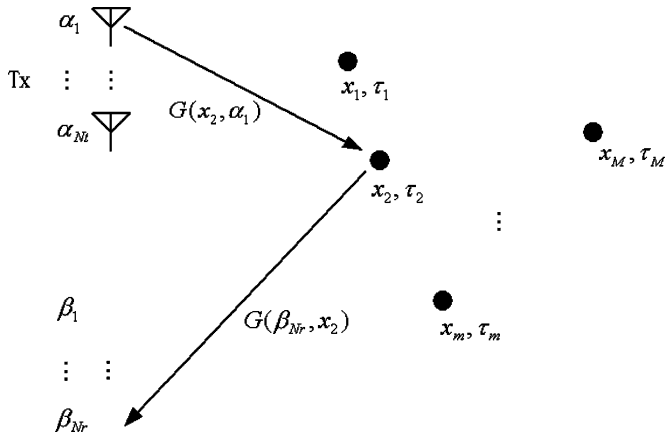


Fig. 1. System setup illustration.

$$\nabla^2 G(\boldsymbol{r}, \boldsymbol{r}', \omega) + (\omega/c_0)^2 n^2(\boldsymbol{x}) G(\boldsymbol{r}, \boldsymbol{r}', \omega) = -\delta(\boldsymbol{r} - \boldsymbol{r}') \quad (1)$$

where $c_0$ is a reference propagation speed and $n(\boldsymbol{x})$ is the refraction index of the medium at position $\boldsymbol{x}$. Though this Green's function is scalar, which is directly applicable to acoustic or ultrasound problems, it could be generalized to the dyadic version [36] when dealing with electromagnetic applications. In the rest of this paper, we will drop the dependence on the frequency $\omega$ in all the notations for the sake of simplicity.

Adopting the Foldy–Lax multiple scattering equations [30]–[32], we formulate the multistatic matrix in [25] and [26] in a closed matrix form as

$$K_{\mathrm{FL}}(\boldsymbol{x}, \boldsymbol{\tau}) = A_r(\boldsymbol{x})[T^{-1}(\boldsymbol{\tau}) - S(\boldsymbol{x})]^{-1} A_t{}^T(\boldsymbol{x}) \quad (2)$$

where "$^T$" stands for a matrix transpose, $\boldsymbol{x}$ is redefined as $\boldsymbol{x} = [\boldsymbol{x}_1^T, \boldsymbol{x}_2^T, \ldots, \boldsymbol{x}_M^T]^T \in \mathbb{R}^{3M}$ representing the unknown scatterer location parameters, $\boldsymbol{\tau} = [\tau_1, \tau_2, \ldots, \tau_M]^T \in \mathbb{C}^M$ unknown scattering parameters, $T(\boldsymbol{\tau}) = \mathrm{diag}\{\boldsymbol{\tau}\}$. The matrix $S(\boldsymbol{x})$ is defined as (3), shown at the bottom of the page, and

$$A_r(\boldsymbol{x}) = [\boldsymbol{g}_r(\boldsymbol{x}_1), \boldsymbol{g}_r(\boldsymbol{x}_2) \cdots \boldsymbol{g}_r(\boldsymbol{x}_M)] \quad (4)$$

$$A_t(\boldsymbol{x}) = [\boldsymbol{g}_t(\boldsymbol{x}_1), \boldsymbol{g}_t(\boldsymbol{x}_2) \cdots \boldsymbol{g}_t(\boldsymbol{x}_M)] \quad (5)$$

$$S(\boldsymbol{x}) = \begin{bmatrix} 0 & G(\boldsymbol{x}_1, \boldsymbol{x}_2) & \cdots & G(\boldsymbol{x}_1, \boldsymbol{x}_M) \\ G(\boldsymbol{x}_2, \boldsymbol{x}_1) & 0 & \cdots & G(\boldsymbol{x}_2, \boldsymbol{x}_M) \\ \vdots & & \ddots & \vdots \\ G(\boldsymbol{x}_{M-1}, \boldsymbol{x}_1) & \cdots & 0 & G(\boldsymbol{x}_{M-1}, \boldsymbol{x}_M) \\ G(\boldsymbol{x}_M, \boldsymbol{x}_1) & \cdots & G(\boldsymbol{x}_M, \boldsymbol{x}_{M-1}) & 0 \end{bmatrix} \quad (3)$$

the receive Green's function vector $\boldsymbol{g}_r(\boldsymbol{x}') \in \mathbb{C}^{N_r}$ as a function of arbitrary location $\boldsymbol{x}' \in \mathbb{R}^3$ is

$$\boldsymbol{g}_r(\boldsymbol{x}') = [G(\boldsymbol{\beta}_1, \boldsymbol{x}'), G(\boldsymbol{\beta}_2, \boldsymbol{x}'), \ldots, G(\boldsymbol{\beta}_{N_r}, \boldsymbol{x}')]^T \quad (6)$$

and the transmit Green's function vector $\boldsymbol{g}_t(\boldsymbol{x}') \in \mathbb{C}^{N_t}$ is

$$\boldsymbol{g}_t(\boldsymbol{x}') = [G(\boldsymbol{x}', \boldsymbol{\alpha}_1), G(\boldsymbol{x}', \boldsymbol{\alpha}_2), \ldots, G(\boldsymbol{x}', \boldsymbol{\alpha}_{N_t})]^T. \quad (7)$$

Since the receive and transmit Green's function vectors incorporate all of the spatial characteristics of the response of the receive and transmit arrays to a point source located at $\boldsymbol{x}'$, they can readily be interpreted as generalizations of the conventional *array response vector* or *steering vector* [11]. Note that the closed-form matrix representation (2) is a function of the background Green's function only.

Theoretically, the matrix $T^{-1}(\boldsymbol{\tau}) - S(\boldsymbol{x})$ may be singular, depending on the setup of the scatterers. For example, this singularity occurs when the matrix pair $(S(\boldsymbol{x}), T^{-1}(\boldsymbol{\tau}))$ has a unit generalized eigenvalue, or equivalently 1 is an eigenvalue of $T(\boldsymbol{\tau})S(\boldsymbol{x})$. In this paper, we consider only the case in which $\rho(T(\boldsymbol{\tau})S(\boldsymbol{x}))$, the spectral radius of $T(\boldsymbol{\tau})S(\boldsymbol{x})$, is strictly less than one, calling it the *weak interaction scattering* case. This condition is satisfied when either the moduli of the scattering potentials $|\tau_m|$, $m = 1, 2, \ldots, M$ are small, the scatterers are sufficiently separated, or both. The *spectral radius* [37] of a matrix $A$ is defined as

$$\rho(A) = \max\{|\lambda| : \lambda \in \mathcal{L}(A)\} \quad (8)$$

where $\mathcal{L}(A)$ is the spectrum of $A$, i.e., the set of eigenvalues of $A$.

Using the identity $(I - A)^{-1} = I + A + A^2 + \cdots$, the multistatic matrix $K_{\mathrm{FL}}(\boldsymbol{x}, \boldsymbol{\tau})$ can be expanded into the power series as

$$\begin{aligned} K_{\mathrm{FL}}(\boldsymbol{x}, \boldsymbol{\tau}) = {} & A_r(\boldsymbol{x})T(\boldsymbol{\tau}){A_t}^T(\boldsymbol{x}) \\ & + A_r(\boldsymbol{x})T(\boldsymbol{\tau})S(\boldsymbol{x})T(\boldsymbol{\tau}){A_t}^T(\boldsymbol{x}) \\ & + A_r(\boldsymbol{x})T(\boldsymbol{\tau})S(\boldsymbol{x})T(\boldsymbol{\tau})S(\boldsymbol{x})T(\boldsymbol{\tau}){A_t}^T(\boldsymbol{x}) + \cdots. \end{aligned} \quad (9)$$

This series form is actually a generalization of the Neumann series or Born series [29], [33], [38] under the multistatic context, and its convergence is guaranteed under our weak scattering assumption $\rho(T(\boldsymbol{\tau})S(\boldsymbol{x})) < 1$. The leading term of (9), known as the Born approximation, represents the first-order scattering, i.e., the scattering without taking into account the multiple scattering. The second term represents the second-order scattering contribution, namely the portion of the scattering that is reflected by the scatterers exactly twice. The rest of the series are other higher order scattering terms.

We will employ the Born-approximated model

$$K_B(\boldsymbol{x}, \boldsymbol{\tau}) = A_r(\boldsymbol{x})T(\boldsymbol{\tau}){A_t}^T(\boldsymbol{x}) \quad (10)$$

$$= \sum_{m=1}^{M} \tau_m \boldsymbol{g}_r(\boldsymbol{x}_m){\boldsymbol{g}_t}^T(\boldsymbol{x}_m) \quad (11)$$

as the reference model in later sections for studying the effect of multiple scattering on the estimation performance. Observing (11), we can see that the multistatic matrix could be decomposed into $M$ parts that are associated one-to-one with the scattering of the $M$ scatterers. In this case, the scattering is basically modeled as if each scatterer scatters as if it were alone, i.e., there are no interactions among them at all. It is easy to verify that the model (10) is a special case of (2) when the $S(\boldsymbol{x})$ matrix is set to be the zero matrix.

Based on the two physical models (2) and (10) of the multistatic matrix, we investigate the multiple scattering effects on the estimation performance on the location parameters $\boldsymbol{x}$ and scattering parameters $\boldsymbol{\tau}$ of the $M$ point scatterers by conducting CRB analysis. Before computing the CRBs, we further assume that $Y$, the measurement of the multistatic matrix, deviates from the model $K(\boldsymbol{x}, \boldsymbol{\tau})$ by additive independent, identically distributed (i.i.d.) complex circularly symmetric Gaussian noise, i.e.,

$$Y = K(\boldsymbol{x}, \boldsymbol{\tau}) + W \quad (12)$$

where $Y$ is the $N_r \times N_t$ measurement matrix, $W$ is the $N_r \times N_t$ noise matrix whose elements $\mathrm{vec}(W) \sim \mathcal{CN}(\boldsymbol{0}, \sigma^2 I_{N_r N_t})$, $\mathrm{vec}(\cdot)$ stacks the first to the last columns of the matrix one under another to form a long vector, and $I_{N_r N_t}$ is the identity matrix of dimension $N_r N_t \times N_r N_t$. It is worth mentioning that though it is technically feasible to derive the CRBs under a more general correlated noise model, the simple noise model is assumed for gaining insight into the differences between the two scattering effects, i.e., with and without multiple scattering.

## III. CRB Analysis

It is well-known that the CRB [39] limits the performance of any unbiased estimator, and, therefore, provides a fundamental limit on the possible estimation accuracy under the given system setup. It is a local performance bound, tight in large samples and high signal-to-noise (SNR) cases [12]. To quantitatively evaluate the multiple scattering effect, we derive and compare the CRBs on unknown scatterer parameters $\boldsymbol{x}$ and $\boldsymbol{\tau}$ based on the physical models that use the Foldy–Lax model and Born approximation, respectively. Note that model (2) is exact, and (10) is just a first-order approximation of the former. Whereas, in our comparisons, we employ the second model as if it were "exact," we are modeling a fictitious reference scenario where there is ideally no multiple scattering among the scatterers.

Under the noise model defined in Section II, the probability distribution of $Y$ is

$$p(Y; \boldsymbol{x}, \boldsymbol{\tau}, \sigma^2) = \frac{1}{(\pi\sigma^2)^{N_r N_t}} e^{-\|Y - K(\boldsymbol{x}, \boldsymbol{\tau})\|_F^2 / \sigma^2} \quad (13)$$

where $\|\cdot\|_F$ represents the Frobenius norm of a matrix, and the log-likelihood function is

$$l(\boldsymbol{x}, \boldsymbol{\tau}, \sigma^2; Y) = \ln(p(Y; \boldsymbol{x}, \boldsymbol{\tau}, \sigma^2)) \quad (14)$$

where $\ln(\cdot)$ denotes the natural logarithm. We start deriving the CRBs from the expression for the Fisher information matrix (FIM) in [12]. Reparameterizing the unknown scattering parameters $\boldsymbol{\tau}$ into real parameters $\tilde{\boldsymbol{\tau}} = [\Re\{\tau_1\}, \Im\{\tau_1\}, \ldots, \Re\{\tau_M\}, \Im\{\tau_M\}]^T \in \mathbb{R}^{2M}$, where $\Re\{\cdot\}$ and $\Im\{\cdot\}$ denote the

real and imaginary parts of a complex number, respectively. Define $\boldsymbol{\theta} = [\tilde{\boldsymbol{\tau}}^T, \boldsymbol{x}^T]^T$, and the FIM for $\boldsymbol{\theta}$ is found as

$$\begin{aligned}\mathcal{I}(\boldsymbol{\theta}) &= -E\left\{\frac{\partial^2 l(\boldsymbol{x},\boldsymbol{\tau},\sigma^2;Y)}{\partial\boldsymbol{\theta}\partial\boldsymbol{\theta}^T}\right\} \\ &= \frac{2}{\sigma^2}\Re\left\{\left[\frac{\partial \mathrm{vec}(K(\boldsymbol{x},\boldsymbol{\tau}))}{\partial\boldsymbol{\theta}^T}\right]^H\left[\frac{\partial \mathrm{vec}(K(\boldsymbol{x},\boldsymbol{\tau}))}{\partial\boldsymbol{\theta}^T}\right]\right\} \\ &= \frac{2}{\sigma^2}\Re\{D^H(\boldsymbol{\theta})D(\boldsymbol{\theta})\} \end{aligned} \tag{15}$$

where $E\{\cdot\}$ represents expectation and "$H$" the conjugate transpose. Here, the derivative $\partial f/\partial \boldsymbol{a}^T$ is defined as

$$\frac{\partial f}{\partial \boldsymbol{a}^T} = \left[\frac{\partial f}{\partial a_1}, \frac{\partial f}{\partial a_2}, \ldots, \frac{\partial f}{\partial a_m}\right] \tag{16}$$

where $f$ is a scalar function of $\boldsymbol{a} = [a_1, a_2, \ldots, a_m]^T$, and $\partial \boldsymbol{b}/\partial \boldsymbol{a}^T$ is defined as

$$\frac{\partial \boldsymbol{b}}{\partial \boldsymbol{a}^T} = \begin{bmatrix} \frac{\partial b_1}{\partial a_1} & \cdots & \frac{\partial b_1}{\partial a_m} \\ \vdots & & \vdots \\ \frac{\partial b_n}{\partial a_1} & \cdots & \frac{\partial b_n}{\partial a_m} \end{bmatrix} \tag{17}$$

where $\boldsymbol{b} = [b_1, b_2, \ldots, b_n]^T$. Note that the noise parameter $\sigma^2$ is disjoint (block diagonal) with the location and scattering parameters $\boldsymbol{x}$ and $\tilde{\boldsymbol{\tau}}$ in full FIM of $\boldsymbol{x}$, $\tilde{\boldsymbol{\tau}}$ and $\sigma^2$. We here work on the FIM of the $\boldsymbol{x}$ and $\tilde{\boldsymbol{\tau}}$ only. The Jacobian matrix

$$D(\boldsymbol{\theta}) = \frac{\partial \mathrm{vec}(K(\boldsymbol{x},\boldsymbol{\tau}))}{\partial \boldsymbol{\theta}^T} \tag{18}$$

could be further partitioned as

$$D(\boldsymbol{\theta}) = [D_{\tilde{\boldsymbol{\tau}}}, D_{\boldsymbol{x}}] \tag{19}$$

where

$$D_{\tilde{\boldsymbol{\tau}}} = \frac{\partial \mathrm{vec}(K(\boldsymbol{x},\boldsymbol{\tau}))}{\partial \tilde{\boldsymbol{\tau}}^T} \tag{20}$$

$$D_{\boldsymbol{x}} = \frac{\partial \mathrm{vec}(K(\boldsymbol{x},\boldsymbol{\tau}))}{\partial \boldsymbol{x}^T}. \tag{21}$$

Following the previous partition, the FIM is partitioned accordingly as

$$\mathcal{I}(\boldsymbol{\theta}) = \begin{bmatrix} \mathcal{I}_{\tilde{\boldsymbol{\tau}}\tilde{\boldsymbol{\tau}}} & \mathcal{I}_{\boldsymbol{x}\tilde{\boldsymbol{\tau}}}^T \\ \mathcal{I}_{\boldsymbol{x}\tilde{\boldsymbol{\tau}}} & \mathcal{I}_{\boldsymbol{x}\boldsymbol{x}} \end{bmatrix}. \tag{22}$$

The CRB matrix for $\tilde{\boldsymbol{\tau}}$ and $\boldsymbol{x}$ is found as the inverse of the FIM, i.e.,

$$\begin{aligned}\mathrm{CRB}(\boldsymbol{\theta}) &= \begin{bmatrix} \mathcal{I}_{\tilde{\boldsymbol{\tau}}\tilde{\boldsymbol{\tau}}} & \mathcal{I}_{\boldsymbol{x}\tilde{\boldsymbol{\tau}}}^T \\ \mathcal{I}_{\boldsymbol{x}\tilde{\boldsymbol{\tau}}} & \mathcal{I}_{\boldsymbol{x}\boldsymbol{x}} \end{bmatrix}^{-1} \\ &= \begin{bmatrix} \mathrm{CRB}_{\tilde{\boldsymbol{\tau}}\tilde{\boldsymbol{\tau}}} & \mathrm{CRB}_{\boldsymbol{x}\tilde{\boldsymbol{\tau}}}^T \\ \mathrm{CRB}_{\boldsymbol{x}\tilde{\boldsymbol{\tau}}} & \mathrm{CRB}_{\boldsymbol{x}\boldsymbol{x}} \end{bmatrix}. \end{aligned} \tag{23}$$

The CRB matrix for location parameters $\boldsymbol{x}$ corresponds to the lower right block of the CRB matrix

$$\mathrm{CRB}(\boldsymbol{x};\tilde{\boldsymbol{\tau}}) = \mathrm{CRB}_{\boldsymbol{x}\boldsymbol{x}} = (\mathcal{I}_{\boldsymbol{x}\boldsymbol{x}} - \mathcal{I}_{\boldsymbol{x}\tilde{\boldsymbol{\tau}}}\mathcal{I}_{\tilde{\boldsymbol{\tau}}\tilde{\boldsymbol{\tau}}}^{-1}\mathcal{I}_{\boldsymbol{x}\tilde{\boldsymbol{\tau}}}^T)^{-1} \tag{24}$$

by the partitioned inverse identity [40]. Similarly, the CRB matrix for scattering parameter $\tilde{\boldsymbol{\tau}}$ is

$$\mathrm{CRB}(\tilde{\boldsymbol{\tau}};\boldsymbol{x}) = \mathrm{CRB}_{\tilde{\boldsymbol{\tau}}\tilde{\boldsymbol{\tau}}} = (\mathcal{I}_{\tilde{\boldsymbol{\tau}}\tilde{\boldsymbol{\tau}}} - \mathcal{I}_{\boldsymbol{x}\tilde{\boldsymbol{\tau}}}^T\mathcal{I}_{\boldsymbol{x}\boldsymbol{x}}^{-1}\mathcal{I}_{\boldsymbol{x}\tilde{\boldsymbol{\tau}}})^{-1}. \tag{25}$$

We define

$$\mathcal{I}(\boldsymbol{x};\tilde{\boldsymbol{\tau}}) = \mathcal{I}_{\boldsymbol{x}\boldsymbol{x}} - \mathcal{I}_{\boldsymbol{x}\tilde{\boldsymbol{\tau}}}\mathcal{I}_{\tilde{\boldsymbol{\tau}}\tilde{\boldsymbol{\tau}}}^{-1}\mathcal{I}_{\boldsymbol{x}\tilde{\boldsymbol{\tau}}}^T \tag{26}$$

which is the Schur complement [40] of $\mathcal{I}_{\tilde{\boldsymbol{\tau}}\tilde{\boldsymbol{\tau}}}$ in $\mathcal{I}(\boldsymbol{\theta})$, as the FIM of $\boldsymbol{x}$ in the presence of nuisance parameter $\tilde{\boldsymbol{\tau}}$, in respect that $\mathrm{CRB}(\boldsymbol{x};\tilde{\boldsymbol{\tau}}) = \mathcal{I}(\boldsymbol{x};\tilde{\boldsymbol{\tau}})^{-1}$. Note that $\mathcal{I}_{\boldsymbol{x}\boldsymbol{x}}$ represents the Fisher information of $\boldsymbol{x}$ with *a prior* known $\tilde{\boldsymbol{\tau}}$, it is not surprising to see that $\mathcal{I}_{\boldsymbol{x}\boldsymbol{x}} \geq \mathcal{I}(\boldsymbol{x};\tilde{\boldsymbol{\tau}})$ or equivalently $\mathrm{CRB}(\boldsymbol{x};\tilde{\boldsymbol{\tau}}) \geq \mathcal{I}_{\boldsymbol{x}\boldsymbol{x}}^{-1}$, where $A \geq B$ for matrices $A$ and $B$ means that $A - B$ is nonnegative definite. The difference of the two FIMs $\mathcal{I}_{\boldsymbol{x}\boldsymbol{x}} - \mathcal{I}(\boldsymbol{x};\tilde{\boldsymbol{\tau}}) = \mathcal{I}_{\boldsymbol{x}\tilde{\boldsymbol{\tau}}}\mathcal{I}_{\tilde{\boldsymbol{\tau}}\tilde{\boldsymbol{\tau}}}^{-1}\mathcal{I}_{\boldsymbol{x}\tilde{\boldsymbol{\tau}}}^T$ represents the information loss due to the lack of knowledge on $\tilde{\boldsymbol{\tau}}$. Similarly, the Fisher information matrix of $\tilde{\boldsymbol{\tau}}$ in the presence of nuisance parameter $\boldsymbol{x}$ is defined as

$$\mathcal{I}(\tilde{\boldsymbol{\tau}};\boldsymbol{x}) = \mathcal{I}_{\tilde{\boldsymbol{\tau}}\tilde{\boldsymbol{\tau}}} - \mathcal{I}_{\boldsymbol{x}\tilde{\boldsymbol{\tau}}}^T\mathcal{I}_{\boldsymbol{x}\boldsymbol{x}}^{-1}\mathcal{I}_{\boldsymbol{x}\tilde{\boldsymbol{\tau}}}, \tag{27}$$

and we have $\mathcal{I}_{\tilde{\boldsymbol{\tau}}\tilde{\boldsymbol{\tau}}} \geq \mathcal{I}(\tilde{\boldsymbol{\tau}};\boldsymbol{x})$ and $\mathrm{CRB}(\tilde{\boldsymbol{\tau}};\boldsymbol{x}) \geq \mathcal{I}_{\tilde{\boldsymbol{\tau}}\tilde{\boldsymbol{\tau}}}^{-1}$.

The CRB (24) could be achieved asymptotically by the maximum likelihood (ML) estimator [12] that jointly estimates $\boldsymbol{x}$ and $\boldsymbol{\tau}$ or by the estimator that maximizes the likelihood function concentrated with respect to the nuisance parameter. In fact, the CRB (24) will coincide with the concentrated CRB derived from such a concentrated likelihood function. The proof is based on a similar approach to that employed in [41] and will not be presented here.

### A. CRBs for the Case With Multiple Scattering

Using the identity $\mathrm{vec}(ADB) = (B^T \otimes A)\mathrm{vec}D$ [42], the vectorized multistatic matrix model (2) using the Foldy–Lax multiple scattering model is

$$\mathrm{vec}(K_{\mathrm{FL}}(\boldsymbol{x},\boldsymbol{\tau})) = [A_t(\boldsymbol{x}) \otimes A_r(\boldsymbol{x})]\mathrm{vec}([T^{-1}(\boldsymbol{\tau}) - S(\boldsymbol{x})]^{-1}).$$

The Jacobian matrices $D_{\mathrm{FL}\tilde{\boldsymbol{\tau}}}$ and $D_{\mathrm{FL}\boldsymbol{x}}$ are found as

$$\begin{aligned} D_{\mathrm{FL}\tilde{\boldsymbol{\tau}}} &= (A_t(\boldsymbol{x})[I_M - T(\boldsymbol{\tau})S(\boldsymbol{x})]^{-1} \\ &\quad \odot A_r(\boldsymbol{x})[I_M - T(\boldsymbol{\tau})S(\boldsymbol{x})]^{-1}) \otimes [1, i] \end{aligned} \tag{28}$$

$$\begin{aligned} D_{\mathrm{FL}\boldsymbol{x}} &= (A_t(\boldsymbol{x})[T^{-1}(\boldsymbol{\tau}) - S(\boldsymbol{x})]^{-1} \otimes \mathbf{1}_n^T) \odot B_r(\boldsymbol{x}) \\ &\quad - \left(A_t(\boldsymbol{x})[T^{-1}(\boldsymbol{\tau}) - S(\boldsymbol{x})]^{-1}\right. \\ &\quad \left.\otimes A_r(\boldsymbol{x})[T^{-1}(\boldsymbol{\tau}) - S(\boldsymbol{x})]^{-1}\right) C(\boldsymbol{x}) \\ &\quad + B_t(\boldsymbol{x}) \odot \left(A_r(\boldsymbol{x})[T^{-1}(\boldsymbol{\tau}) - S(\boldsymbol{x})]^{-1} \otimes \mathbf{1}_n^T\right) \end{aligned} \tag{29}$$

where

- "$\otimes$" represents the Kronecker product [42];
- "$\odot$" stands for the Khatri–Rao product[1] [42];
- "$i$" is the imaginary unit;
- $B_t(\boldsymbol{x}) = [\boldsymbol{b}_t(\boldsymbol{x}_1), \boldsymbol{b}_t(\boldsymbol{x}_2) \cdots \boldsymbol{b}_t(\boldsymbol{x}_M)]$;
- $\boldsymbol{b}_t(\boldsymbol{x}_m) = \partial \boldsymbol{g}_t(\boldsymbol{x}_m)/\partial \boldsymbol{x}_m^T$, $m = 1, 2, \ldots, M$;
- $B_r(\boldsymbol{x}) = [\boldsymbol{b}_r(\boldsymbol{x}_1), \boldsymbol{b}_r(\boldsymbol{x}_2) \cdots \boldsymbol{b}_r(\boldsymbol{x}_M)]$;
- $\boldsymbol{b}_r(\boldsymbol{x}_m) = \partial \boldsymbol{g}_r(\boldsymbol{x}_m)/\partial \boldsymbol{x}_m^T$, $m = 1, 2, \ldots, M$;

[1]The Khatri–Rao product of two matrices with the same number of columns is defined as $A \odot B = [\boldsymbol{a}_1 \otimes \boldsymbol{b}_1, \boldsymbol{a}_2 \otimes \boldsymbol{b}_2 \cdots \boldsymbol{a}_n \otimes \boldsymbol{b}_n]$, where $A = [\boldsymbol{a}_1, \boldsymbol{a}_2 \cdots \boldsymbol{a}_n]$ and $B = [\boldsymbol{b}_1, \boldsymbol{b}_2 \cdots \boldsymbol{b}_n]$.

- $\mathbf{1}_n$: $n$-dimension column vector with each element as 1;
- $n$ is the dimension of one location parameter $\boldsymbol{x}_m$, for example, $n = 3$ when solving the problem in a general 3-D space;
- $C(\boldsymbol{x}) = [\boldsymbol{c}^T(\boldsymbol{x}_1), \boldsymbol{c}^T(\boldsymbol{x}_2) \cdots \boldsymbol{c}^T(\boldsymbol{x}_M)]^T$;
- $\boldsymbol{c}(\boldsymbol{x}_m) = \partial \boldsymbol{g}(\boldsymbol{x}_m)/\partial \boldsymbol{x}^T$, $m = 1, 2, \ldots, M$;
- $\boldsymbol{g}(\boldsymbol{x}_m) = [G(\boldsymbol{x}_1, \boldsymbol{x}_m), G(\boldsymbol{x}_2, \boldsymbol{x}_m), \ldots, G(\boldsymbol{x}_M, \boldsymbol{x}_m)]^T$, in which $G(\boldsymbol{x}_m, \boldsymbol{x}_m) \triangleq 0$, $m = 1, 2, \ldots, M$.

*Proof:* See Appendix A.

To compute the $\mathrm{CRB}_{\mathrm{FL}}(\boldsymbol{x}; \tilde{\boldsymbol{\tau}})$ and $\mathrm{CRB}_{\mathrm{FL}}(\tilde{\boldsymbol{\tau}}; \boldsymbol{x})$, we first compute $D_{\mathrm{FL}\tilde{\boldsymbol{\tau}}}$ and $D_{\mathrm{FL}\boldsymbol{x}}$ as previously shown and substitute them into (15) for the FIM and then (24) and (25) for the CRBs of $\boldsymbol{x}$ and $\tilde{\boldsymbol{\tau}}$.

### *B. CRBs for the Reference Case With No Multiple Scattering*

For the reference case, namely without multiple scattering, we use the multistatic model (10) based on the Born approximation, which models a fictitious reference scenario where there is ideally no multiple scattering. Then the vectorized version of the multistatic matrix model (10) is

$$\mathrm{vec}(K_{\mathrm{B}}(\boldsymbol{x}, \boldsymbol{\tau})) = [A_t(\boldsymbol{x}) \odot A_r(\boldsymbol{x})]\boldsymbol{\tau} \tag{30}$$

where we used the identity $\mathrm{vec}(\mathrm{AVD}) = (D^T \odot A)\mathrm{vecd}(V)$ [42], where $V$ is diagonal and $\mathrm{vecd}(\cdot)$ forms a vector from the diagonal elements of the matrix. Recalling that multistatic model (10) is the special case of (2) when $S(\boldsymbol{x})$ is the zero matrix, we can find the Jacobian matrices $D_{\mathrm{B}\tilde{\boldsymbol{\tau}}}$ and $D_{\mathrm{B}\boldsymbol{x}}$ simply by substituting $S(\boldsymbol{x})$ as a zero matrix into (28) and (29), which are

$$D_{\mathrm{B}\tilde{\boldsymbol{\tau}}} = A_t(\boldsymbol{x}) \odot A_r(\boldsymbol{x}) \otimes [1, i] \tag{31}$$

$$D_{\mathrm{B}\boldsymbol{x}} = \left[A_t(\boldsymbol{x}) T(\boldsymbol{\tau}) \otimes \mathbf{1}_n^T\right] \odot B_r(\boldsymbol{x}) + B_t(\boldsymbol{x}) \odot \left[A_r(\boldsymbol{x}) T(\boldsymbol{\tau}) \otimes \mathbf{1}_n^T\right]. \tag{32}$$

Then, $\mathrm{CRB}_{\mathrm{B}}(\boldsymbol{x}; \tilde{\boldsymbol{\tau}})$ and $\mathrm{CRB}_{\mathrm{B}}(\tilde{\boldsymbol{\tau}}; \boldsymbol{x})$ could be subsequently computed from $D_{\mathrm{B}\tilde{\boldsymbol{\tau}}}$ and $D_{\mathrm{B}\boldsymbol{x}}$.

## IV. Numerical Analysis of the Multiple Scattering

In this section, we present numerical comparisons of the CRBs computed by the Foldy–Lax multiple scattering model and the Born approximation, respectively. We assume that the background is homogeneous; then for each scatterer, the other scatterers behave as part of the background and induce inhomogeneity by multiple scattering. For the reference case without multiple scattering, the setup for each scatterer is just homogeneous. Thus, the inhomogeneity is due solely to the multiple scattering, and its effect is evaluated by comparing the CRBs of scatterer parameters for the two cases. It is worth emphasizing that we assume both the Foldy–Lax and Born approximation physical models are exact in the computation and comparison of the CRBs, i.e., there is no modeling error issue involved. In other words, the two physical models represent two distinct physical processes, and we wish to evaluate the multiple scattering, the difference between them, in terms of its effect on the estimation performance bounds.

We consider the 2-D setup: the antenna elements and scatterers are infinite lines and perpendicular to the $x$–$y$ plane; then the locations of targets and antennas could be represented mathematically as points in the $x$–$y$ plane. The background Green's function for the 2-D case [36], [43] is

$$G(\boldsymbol{r}, \boldsymbol{r}') = \frac{i}{4} H_0(2\pi|\boldsymbol{r} - \boldsymbol{r}'|/\lambda) \tag{33}$$

where $H_0$ is the zero-order Hankel function of the first kind, which could be approximated under a far field assumption [43] as

$$G(\boldsymbol{r}, \boldsymbol{r}') \approx \frac{i}{4}\sqrt{\frac{2}{\pi}} \frac{e^{i2\pi|\boldsymbol{r}-\boldsymbol{r}'|/\lambda}}{\sqrt{2\pi|\boldsymbol{r} - \boldsymbol{r}'|/\lambda}} e^{-i\pi/4}. \tag{34}$$

For computing CRBs analytically, we use the approximate form and drop the unessential constant. The background Green's function used in the following numerical examples is:

$$G(\boldsymbol{r}, \boldsymbol{r}') = \frac{e^{i2\pi|\boldsymbol{r}-\boldsymbol{r}'|/\lambda}}{\sqrt{2\pi|\boldsymbol{r} - \boldsymbol{r}'|/\lambda}}. \tag{35}$$

When computing the Jacobian matrices (20) and (21) and (31) and (32), the derivatives of Green's functions with respect to the location parameters are found as

$$\frac{\partial G(\boldsymbol{x}_m, \boldsymbol{\alpha}_k)}{\partial \boldsymbol{x}_m} = G(\boldsymbol{x}_m, \boldsymbol{\alpha}_k) \frac{\frac{i2\pi}{\lambda}|\boldsymbol{x}_m - \boldsymbol{\alpha}_k| - \frac{1}{2}}{|\boldsymbol{x}_m - \boldsymbol{\alpha}_k|^2} (\boldsymbol{x}_m - \boldsymbol{\alpha}_k) \tag{36}$$

where $k = 1, 2, \ldots, N_t$, $m = 1, 2, \ldots, M$ and

$$\frac{\partial \boldsymbol{g}_t(\boldsymbol{x}_m)}{\partial \boldsymbol{x}_m^T} = \left[\frac{\partial G(\boldsymbol{x}_m, \boldsymbol{\alpha}_1)}{\partial \boldsymbol{x}_m} \cdots \frac{\partial G(\boldsymbol{x}_m, \boldsymbol{\alpha}_{N_t})}{\partial \boldsymbol{x}_m}\right]^T. \tag{37}$$

Similarly

$$\frac{\partial G(\boldsymbol{\beta}_j, \boldsymbol{x}_m)}{\partial \boldsymbol{x}_m} = G(\boldsymbol{\beta}_j, \boldsymbol{x}_m) \frac{\frac{i2\pi}{\lambda}|\boldsymbol{x}_m - \boldsymbol{\beta}_j| - \frac{1}{2}}{|\boldsymbol{x}_m - \boldsymbol{\beta}_j|^2} (\boldsymbol{x}_m - \boldsymbol{\beta}_j) \tag{38}$$

where $j = 1, 2, \ldots, N_r$, $m = 1, 2, \ldots, M$, and

$$\frac{\partial \boldsymbol{g}_r(\boldsymbol{x}_m)}{\partial \boldsymbol{x}_m^T} = \left[\frac{\partial G(\boldsymbol{\beta}_1, \boldsymbol{x}_m)}{\partial \boldsymbol{x}_m} \cdots \frac{\partial G(\boldsymbol{\beta}_{N_r}, \boldsymbol{x}_m)}{\partial \boldsymbol{x}_m}\right]^T. \tag{39}$$

See Appendix B for detailed computations.

We employ collocated transmit and receive arrays that are uniform linear arrays (ULAs) located between $(-20, 0)$ and $(20, 0)$ with spacing of 5. Then $N_t = N_r = N = 9$; $\boldsymbol{\alpha}_1 = \boldsymbol{\beta}_1 = (-20, 0)$; $\boldsymbol{\alpha}_2 = \boldsymbol{\beta}_2 = (-15, 0) \ldots \boldsymbol{\alpha}_N = \boldsymbol{\beta}_N = (20, 0)$; and $\boldsymbol{g}_t(\boldsymbol{x}_m) = \boldsymbol{g}_r(\boldsymbol{x}_m)$ for $m = 1, 2, \ldots, M$ and $A_t(\boldsymbol{x}) = A_r(\boldsymbol{x})$. We assume three scatterers are at $(-3, 22)$, $(0, 25)$, and $(3, 22)$, respectively, with unit scattering coefficients. All the coordinates are in the unit of wavelength, i.e., we assume the narrowband signal with $\lambda = 1$. It is well-known that the spatial undersampling will induce grating lobes. We proposed a multiple-frequency scheme for resolving the spatial ambiguity in [25] and [26] for sparse arrays. Though we use the $5\lambda$ antenna spacing for computational simplicity, it is easy to verify that the results on the multiple scattering also hold for transmit and receive arrays with $\lambda/2$ spacing.

In the first example, we demonstrate the CRBs and mean-squared errors (MSEs) of maximum likelihood estimates as a function of the noise level. In Fig. 2, the MSE represents the

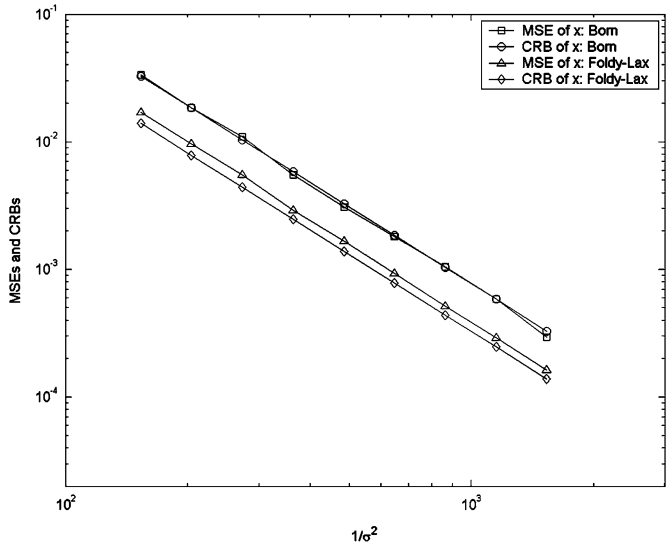


Fig. 2. Sum of MSEs for estimating location parameter $\boldsymbol{x}$, and $\mathrm{trCRB}(\boldsymbol{x};\bar{\boldsymbol{\tau}})$ as a function of noise level.

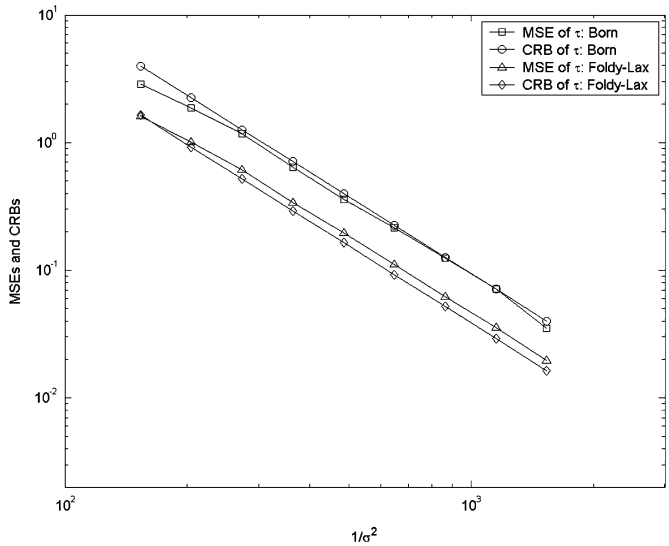


Fig. 3. Sum of MSEs for estimating scattering potential parameter $\bar{\boldsymbol{\tau}}$, and $\mathrm{trCRB}(\tilde{\boldsymbol{\tau}};\boldsymbol{x})$ as a function of noise level.

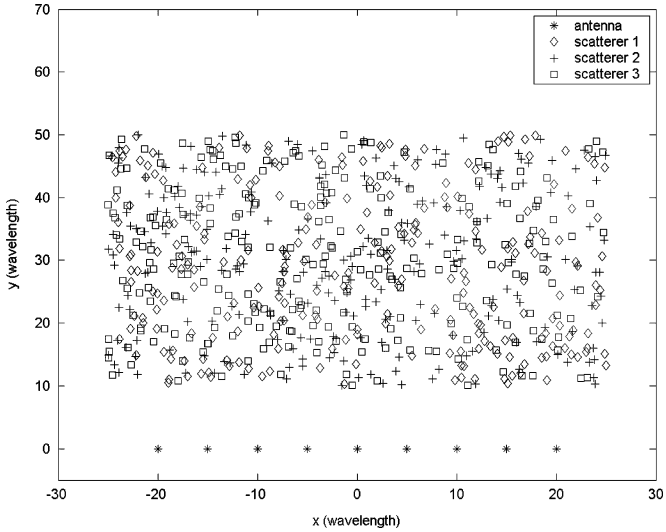


Fig. 4. Scatterer distribution in an example of 251 Monte Carlo runs.

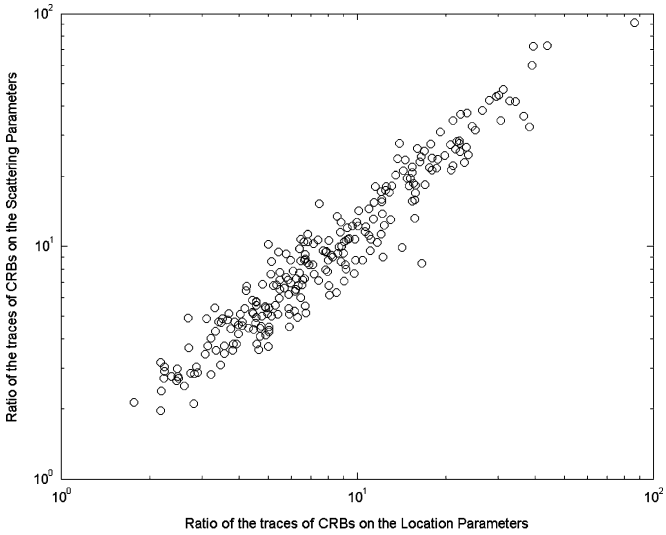


Fig. 5. $\mathrm{trCRB_B}(\bar{\boldsymbol{\tau}};\boldsymbol{x})/\mathrm{trCRB_{FL}}(\bar{\boldsymbol{\tau}};\boldsymbol{x})$ versus $\mathrm{trCRB_B}(\boldsymbol{x};\bar{\boldsymbol{\tau}})/\mathrm{trCRB_{FL}}(\boldsymbol{x};\bar{\boldsymbol{\tau}})$ in the 251 Monte Carlo runs.

sum of the MSEs for the location parameters $\boldsymbol{x}$ and the CRB stands for trace of the CRB matrix on $\boldsymbol{x}$. Fig. 3 demonstrates the sum of the MSEs for the scattering parameter $\tilde{\boldsymbol{\tau}}$ and trace of its CRB matrix. Recall that the Born approximation models the fictitious reference case where there is ideally no multiple scattering; thus, this case may have different received signal power from the case with multiple scattering. In this example, the received signal power with multiple scattering is slightly higher than that without it, which could be intuitively explained by considering that more energy of the incident signals is reflected to the receive array by higher order scatterings [see the physical model (9)]. This improvement, however, is not guaranteed, depending on the scatterer setup, since the scatterings of different orders are added up coherently. Comparing the MSEs with CRBs for the cases with and without multiple scattering, we see that the estimation performance with the multiple scattering is significantly better than without it. Again, this performance improvement might depend on the system setup.

In the second example, we wish to find how the multiple scattering affects the estimation performance under various system setups. We randomize the scatterer setup assuming that scatterers are located uniformly over a rectangular area centered at $(0, 30)$ with dimension $50 \times 40$, and their locations distribute independently. To prevent the scattering from being too weak, the moduli of the scattering potentials are assumed to be independently and uniformly distributed over $[0.5, 1]$, and the phases uniformly distributed over $[0, 2\pi]$. See Fig. 4 for an illustration of the locations of the three scatterers in an example of 251 Monte Carlo runs. To show the effects of multiple scattering at different scatterer setups, we represent each Monte Carlo run in Fig. 5 as one point with $\mathrm{trCRB_B}(\boldsymbol{x};\tilde{\boldsymbol{\tau}})/\mathrm{trCRB_{FL}}(\boldsymbol{x};\tilde{\boldsymbol{\tau}})$ as its $x$ coordinate and $\mathrm{trCRB_B}(\tilde{\boldsymbol{\tau}};\boldsymbol{x})/\mathrm{trCRB_{FL}}(\tilde{\boldsymbol{\tau}};\boldsymbol{x})$ as the $y$ coordinate, where "tr" represents the trace of a matrix. Then, the runs in which the CRBs on $\boldsymbol{x}$ are improved due to the multiple scattering will have the ratio $\mathrm{trCRB_B}(\boldsymbol{x};\tilde{\boldsymbol{\tau}})/\mathrm{trCRB_{FL}}(\boldsymbol{x};\tilde{\boldsymbol{\tau}})$ larger than one,

and those in which the CRBs on $\boldsymbol{x}$ are deteriorated will have ratio less than one. Analogously, the same interpretation applies on the $\mathrm{trCRB_B}(\tilde{\boldsymbol{\tau}};\boldsymbol{x})/\mathrm{trCRB_{FL}}(\tilde{\boldsymbol{\tau}};\boldsymbol{x})$. If we set point $(1,1)$ as the coordinate origin, we can see in Fig. 5 that all of the 251 Monte Carlo runs are located in the first quadrant, which means that multiple scattering improves the CRBs in the randomized setups. The median for $\mathrm{trCRB_B}(\boldsymbol{x};\tilde{\boldsymbol{\tau}})/\mathrm{trCRB_{FL}}(\boldsymbol{x};\tilde{\boldsymbol{\tau}})$ is 7.1254, and 8.6120 for $\mathrm{trCRB_B}(\tilde{\boldsymbol{\tau}};\boldsymbol{x})/\mathrm{trCRB_{FL}}(\tilde{\boldsymbol{\tau}};\boldsymbol{x})$. Obviously the improvement is quite significant. In addition, a strong positive correlation between the two CRB ratios of $\boldsymbol{x}$ and $\boldsymbol{\tau}$ can be seen in Fig. 5, which indicates that the estimation accuracy on the location parameters greatly affects that on the scattering parameters.

Though we have not been able to identify analytical conditions under which multiple scattering is beneficial in terms of improving the CRBs, we find in extensive simulations that the multiple scattering is favorable under most of the weak interaction scattering setups.

## V. Artificial Scatterers

Having shown that multiple scattering can improve estimation performance under certain conditions, in this section we propose the use of artificial scatterers to apply this result.

One way of exploiting the advantage of the multiple scattering is simply to introduce it into the modeling, namely adopting an appropriate physical model to take into account the multiple scattering, which is whereas widely ignored in current literature. Furthermore, we propose the use of *artificial scatterers* to create multiple scattering in the case, for example, with only one target point scatterer in the illuminated scenario, where multiple scattering no longer exists. The multistatic matrix model for this case is reduced to

$$K(\boldsymbol{x}_1,\tau_1)=\tau_1\boldsymbol{g}_r(\boldsymbol{x}_1)\boldsymbol{g}_t{}^T(\boldsymbol{x}_1) \tag{40}$$

where $\boldsymbol{x}_1$ represents the location of the target scatterer and $\tau_1$ is its complex scattering potential. Note that (40) is a special case of both (2) and (10). In [44], we proposed using the artificial scatterers in multiple-input multiple-output (MIMO) wireless communication systems under a macrocell environment to increase its capacity, multiplexing, and diversity gains and to improve the error probability performance. In this paper, we further propose the use of artificial scatterers in the sensing application to create multiple scattering artificially in the hope of improving the estimation performance of system. The artificial scatterers can either be *active* or *passive*: active artificial scatterers could be relays that simply amplify and retransmit the incident wave; passive artificial scatterers could be scatterers that reflect efficiently. The artificial scatterers could be deployed in the scenario of interest in a planned manner or happen to be nearby by opportunity.

Supposing that the locations and scattering potentials of the artificial scatterers are known *a priori*, it is reasonable to project the improvement on the estimation of the target scatterer since the number of unknown parameters is unchanged and the created multiple scattering is very likely helpful. Since the assumption of such *a priori* information may be unrealistic, e.g., for the case in which the artificial scatterers are nearby by opportunity, it is of greater interest to evaluate the effect of artificial scatterers with unknown locations and scattering potentials. We use the following numerical examples to demonstrate the efficacy of the artificial scatterers assuming the locations and scattering potentials of the deployed artificial scatterers are *unknown*.

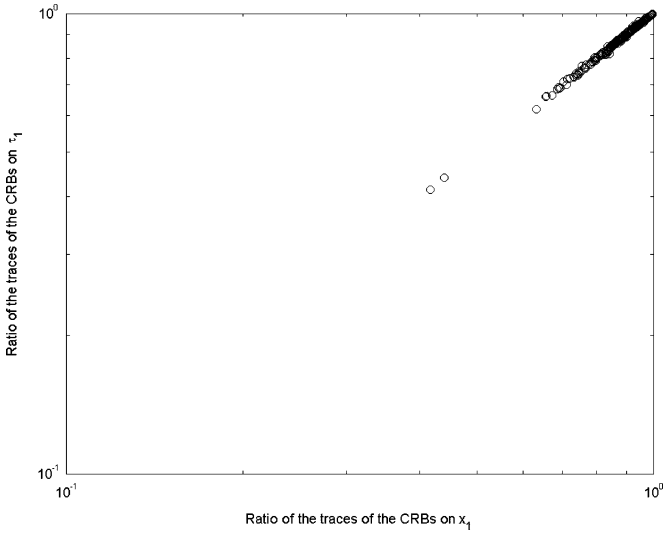


Fig. 6. $\mathrm{trCRB}_1(\bar{\boldsymbol{\tau}}_1)/\mathrm{trCRB}_{1+2}(\bar{\boldsymbol{\tau}}_1)$ versus $\mathrm{trCRB}_1(\boldsymbol{x}_1)/\mathrm{trCRB}_{1+2}(\boldsymbol{x}_1)$ in the absence of multiple scattering.

We assume the same transmit and receive arrays as in the examples of Section IV, with one target scatterer and two artificial scatterers uniformly and independently distributed within the same rectangular region as those in example 2 of Section IV. The moduli of the scattering potentials of the target scatterer and two artificial scatterers are independently and uniformly distributed over $[0.5,1]$, and the phases uniformly distributed over $[0,2\pi]$. We compute the traces of the CRBs on the location $\boldsymbol{x}_1$ and scattering parameters $\tau_1$ of the target scatterer for the case without artificial scatterers, denoted by $\mathrm{trCRB}_1(\boldsymbol{x}_1)$ and $\mathrm{trCRB}_1(\tilde{\boldsymbol{\tau}}_1)$, respectively, where $\tilde{\boldsymbol{\tau}}_1=[\Re\{\tau_1\},\Im\{\tau_1\}]^T$, then compute the traces of the CRBs of the target scatterer after deploying two artificial scatterers, denoted by $\mathrm{trCRB}_{1+2}(\boldsymbol{x}_1)$ and $\mathrm{trCRB}_{1+2}(\tilde{\boldsymbol{\tau}}_1)$. We plot the Monte Carlo runs with $\mathrm{trCRB}_1(\boldsymbol{x}_1)/\mathrm{trCRB}_{1+2}(\boldsymbol{x}_1)$ as $x$ coordinates and $\mathrm{trCRB}_1(\tilde{\boldsymbol{\tau}}_1)/\mathrm{trCRB}_{1+2}(\tilde{\boldsymbol{\tau}}_1)$ as $y$ coordinates. In Fig. 6, the CRBs are computed using the Born approximated model (10); it is not surprising to see that all the runs appear in the third quadrant, which means that the added artificial scatterers decrease the estimation performance of the target scatterer in the case without multiple scattering. This decrease in estimation performance is the direct result of the increasing of unknown parameters, thus reducing the degrees of freedom of the estimation problem. In Fig. 7, the CRBs are computed using the Foldy–Lax multiple scattering model (2). It is quite interesting to find that 204 out of the 251 Monte Carlo runs lie in the first quadrant in this case, meaning that the two randomly deployed artificial scatterers improved the estimation performance on the target scatterer via the created multiple scattering. The median for $\mathrm{trCRB}_1(\boldsymbol{x}_1)/\mathrm{trCRB}_{1+2}(\boldsymbol{x}_1)$ is 6.6418, and 7.9206 for $\mathrm{trCRB}_1(\tilde{\boldsymbol{\tau}}_1)/\mathrm{trCRB}_{1+2}(\tilde{\boldsymbol{\tau}}_1)$. The

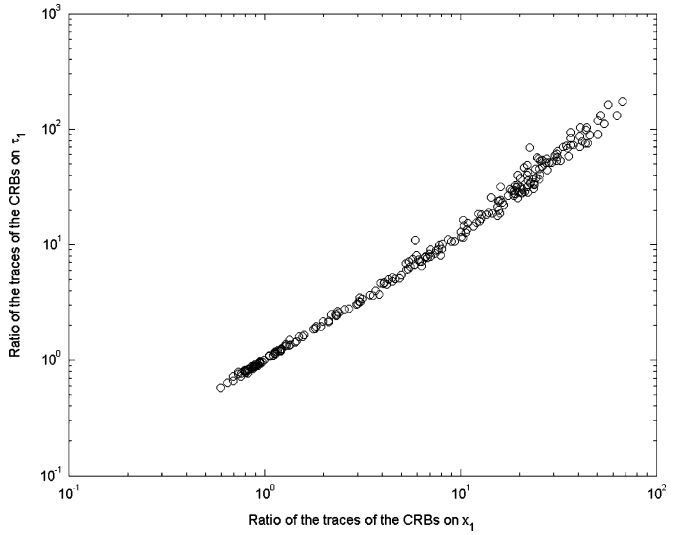


Fig. 7. $\mathrm{trCRB}_1(\bar{\boldsymbol{\tau}}_1)/\mathrm{trCRB}_{1+2}(\bar{\boldsymbol{\tau}}_1)$ versus $\mathrm{trCRB}_1(\boldsymbol{x}_1)/\mathrm{trCRB}_{1+2}(\boldsymbol{x}_1)$ in the presence of multiple scattering.

multiple scattering surprisingly not only offsets the degradation of the CRBs on the target scatterers due the lowered degrees of freedoms, but also improves the estimation performance further in most of the randomized scatterer setups.

## VI. Conclusion

We derived the CRBs on the location and scattering parameters of point scatterers under a multistatic sensing setup for the cases in which multiple scattering either exist or not. We demonstrated that the inhomogeneity induced by the multiple scattering could greatly improve the estimation performance in terms of the CRBs. Higher order scattering components actually contain much richer information about the scatterers compared with the first order scattering component. We then proposed to use artificial scatterers in the absence of multiple scattering. Interestingly, the multiple scattering created by these artificial scatterers could improve the estimation performance despite the decreased degrees of freedom by the unknown parameters of the artificial scatterers.

Analytically comparing the CRB expression in terms of their trace, determinant, or any matrix norm is challenging due to the nonlinear dependence of the CRB matrices on the system parameters. We will investigate this problem in our future work. Also, since the effect of multiple scattering depends on system setup, identifying the conditions under which multiple scattering is favorable is of great interest, which will also be considered in our future work.

## Appendix A

We present detailed steps for computing the Jacobian matrices $D_{\mathrm{FL}\tilde{\boldsymbol{\tau}}}$ and $D_{\mathrm{FL}\boldsymbol{x}}$ based on the multistatic matrix (2) that uses the Foldy–Lax multiple scattering model. The following computations use the derivative of a matrix with respective to another matrix. Among the many different definitions available, we use the one suggested in [45], i.e.,

$$\frac{\partial A}{\partial B}=\frac{\partial \mathrm{vec}(A)}{\partial \mathrm{vec}(B)^T}. \tag{A1}$$

It is easy to verify that the chain rule holds under such a definition

$$\frac{\partial A}{\partial C}=\frac{\partial \mathrm{vec}(A)}{\partial \mathrm{vec}(C)^T}=\frac{\partial \mathrm{vec}(A)}{\partial \mathrm{vec}(B)^T}\frac{\partial \mathrm{vec}(B)}{\partial \mathrm{vec}(C)^T}=\frac{\partial A}{\partial B}\frac{\partial B}{\partial C}. \tag{A2}$$

For the derivative involving complex independent variables, we use the generalized definition of a complex derivative defined in [46]–[48]

$$\frac{df(z)}{dz}=\frac{1}{2}\left(\frac{\partial f(z)}{\partial \Re\{z\}}-i\frac{\partial f(z)}{\partial \Im\{z\}}\right) \tag{A3}$$

where $z$ is the complex independent variable and $f(z)$ is a scalar function of $z$. It is well-known that if the complex function $f(z)$ is *analytic* or *complex differentiable* in a region $R$, it satisfies the Cauchy–Riemann equations

$$\frac{df(z)}{dz}=\frac{\partial \Re\{f(z)\}}{\partial \Re\{z\}}+i\frac{\partial \Im\{f(z)\}}{\partial \Re\{z\}} \tag{A4}$$

$$=-i\frac{\partial \Re\{f(z)\}}{\partial \Im\{z\}}+\frac{\partial \Im\{f(z)\}}{\partial \Im\{z\}} \tag{A5}$$

for every point in this region. For analytic functions, the regular chain rule applies [48]

$$\frac{\partial f(u)}{\partial z}=\frac{\partial f}{\partial u}\frac{\partial u}{\partial z}. \tag{A6}$$

In the following derivations, we basically use two classes of complex functions: the linear function $f_1(z)=az+b$, which is holomorphic, and $f_2(z)=(cz+d)/(az+b)$, which is meromorphic. Thus, the chain rule holds for complex derivatives involving these two functions except at discrete singular points.

*Derivation of* $D_{\mathrm{FL}\tilde{\boldsymbol{\tau}}}$

$$\begin{aligned}
D_{\mathrm{FL}\tilde{\boldsymbol{\tau}}}&=\frac{\partial \mathrm{vec}(K_{\mathrm{FL}}(\boldsymbol{x},\boldsymbol{\tau}))}{\partial \tilde{\boldsymbol{\tau}}^T}\\
&=\frac{\partial \mathrm{vec}(K_{\mathrm{FL}}(\boldsymbol{x},\boldsymbol{\tau}))}{\partial \boldsymbol{\tau}^T}\otimes[1,i]\\
&=\frac{\partial}{\partial \boldsymbol{\tau}^T}[(A_t(\boldsymbol{x})\otimes A_r(\boldsymbol{x}))\mathrm{vec}([T^{-1}(\boldsymbol{\tau})-S(\boldsymbol{x})]^{-1})]\\
&\quad\otimes[1,i]\\
&=(A_t(\boldsymbol{x})\otimes A_r(\boldsymbol{x}))\frac{\partial}{\partial \boldsymbol{\tau}^T}\mathrm{vec}([T^{-1}(\boldsymbol{\tau})-S(\boldsymbol{x})]^{-1})\\
&\quad\otimes[1,i]\\
&=-(A_t(\boldsymbol{x})\otimes A_r(\boldsymbol{x}))([T^{-1}(\boldsymbol{\tau})-S(\boldsymbol{x})]^{-1}\\
&\quad\otimes[T^{-1}(\boldsymbol{\tau})-S(\boldsymbol{x})]^{-1})\frac{\partial}{\partial \boldsymbol{\tau}^T}\mathrm{vec}(T^{-1}(\boldsymbol{\tau})-S(\boldsymbol{x}))\\
&\quad\otimes[1,i]\\
&=-(A_t(\boldsymbol{x})[T^{-1}(\boldsymbol{\tau})-S(\boldsymbol{x})]^{-1}\\
&\quad\otimes A_r(\boldsymbol{x})[T^{-1}(\boldsymbol{\tau})-S(\boldsymbol{x})]^{-1})\frac{\partial}{\partial \boldsymbol{\tau}^T}\mathrm{vec}(T^{-1}(\boldsymbol{\tau}))\\
&\quad\otimes[1,i]\\
&=-(A_t(\boldsymbol{x})[T^{-1}(\boldsymbol{\tau})-S(\boldsymbol{x})]^{-1}\\
&\quad\otimes A_r(\boldsymbol{x})[T^{-1}(\boldsymbol{\tau})-S(\boldsymbol{x})]^{-1})J_M\frac{\partial}{\partial \boldsymbol{\tau}^T}\mathrm{vecd}(T^{-1}(\boldsymbol{\tau}))\\
&\quad\otimes[1,i]\\
&=-(A_t(\boldsymbol{x})[T^{-1}(\boldsymbol{\tau})-S(\boldsymbol{x})]^{-1}\\
&\quad\odot A_r(\boldsymbol{x})[T^{-1}(\boldsymbol{\tau})-S(\boldsymbol{x})]^{-1})\frac{\partial}{\partial \boldsymbol{\tau}^T}\mathrm{vecd}(T^{-1}(\boldsymbol{\tau}))\\
&\quad\otimes[1,i]
\end{aligned}$$

$$
\begin{aligned}
&= (A_t(\boldsymbol{x})[T^{-1}(\boldsymbol{\tau}) - S(\boldsymbol{x})]^{-1} \odot A_r(\boldsymbol{x})[T^{-1}(\boldsymbol{\tau}) \\
&\quad - S(\boldsymbol{x})]^{-1})T^{-1}(\boldsymbol{\tau})T^{-1}(\boldsymbol{\tau}) \otimes [1, i] \\
&= (A_t(\boldsymbol{x})[T^{-1}(\boldsymbol{\tau}) - S(\boldsymbol{x})]^{-1}T^{-1}(\boldsymbol{\tau}) \\
&\quad \odot A_r(\boldsymbol{x})[T^{-1}(\boldsymbol{\tau}) - S(\boldsymbol{x})]^{-1}T^{-1}(\boldsymbol{\tau})) \otimes [1, i] \\
&= (A_t(\boldsymbol{x})[I_M - T(\boldsymbol{\tau})S(\boldsymbol{x})]^{-1} \\
&\quad \odot A_r(\boldsymbol{x})[I_M - T(\boldsymbol{\tau})S(\boldsymbol{x})]^{-1}) \otimes [1, i].
\end{aligned}
$$

In the second equality, we used $\mathrm{d}\tau_m = \mathrm{d}\Re\{\tau_m\} + i\mathrm{d}\Im\{\tau_m\}$, where $m = 1, 2, \ldots, M$. In the fifth equality, we used the identity $\partial \mathrm{vec}(X^{-1})/\partial \mathrm{vec}(X)^T = -(X^T)^{-1} \otimes X^{-1}$ [45]. In the sixth equality, we used $(A \otimes B)(C \otimes D) = AC \otimes BD$ [42]. In the seventh equality, we used $\mathrm{vec}(A) = J_M \mathrm{vecd}(A)$ [49], where $A$ is a diagonal matrix of dimension $M \times M$, $J_M$ is a $M^2 \times M$ selection matrix [49] defined as

$$
J_M = I_M \odot I_M = [e_1 \otimes e_1, e_2 \otimes e_2 \cdots e_M \otimes e_M] \tag{A7}
$$

and $e_m$ is a $M \times 1$ column vector with 1 in the $m$th position and zeros elsewhere, i.e.,

$$
e_m = [\underbrace{0 \cdots 01}_{m} 0 \cdots 0]^T, 1 \le m \le M. \tag{A8}
$$

In the eighth equality we used the identity $(A \otimes B)J_M = (A \otimes B)(I_M \odot I_M) = A \odot B$ [49], [42]. In the ninth equality, we used $\partial \mathrm{vecd}(T^{-1}(\boldsymbol{\tau}))/\partial \boldsymbol{\tau}^T = -T^{-1}(\boldsymbol{\tau})T^{-1}(\boldsymbol{\tau})$, and the tenth equality is easily verified. □

*Derivation of* $D_{\mathrm{FL}}\boldsymbol{x}$

$$
\begin{aligned}
D_{\mathrm{FL}x} &= \frac{\partial \mathrm{vec}(K_{\mathrm{FL}}(\boldsymbol{x}, \boldsymbol{\tau}))}{\partial \boldsymbol{x}^T} \\
&= \frac{\partial}{\partial \boldsymbol{x}^T} \mathrm{vec}(A_r(\boldsymbol{x})[T^{-1}(\boldsymbol{\tau}) - S(\boldsymbol{x})]^{-1} {A_t}^T(\boldsymbol{x})) \\
&= (A_t(\boldsymbol{x})[T^{-1}(\boldsymbol{\tau}) - S(\boldsymbol{x})]^{-1} \otimes I_{N_r}) \frac{\partial \mathrm{vec}(A_r(\boldsymbol{x}))}{\partial \boldsymbol{x}^T} \\
&\quad - (A_t(\boldsymbol{x})[T^{-1}(\boldsymbol{\tau}) - S(\boldsymbol{x})]^{-1} \\
&\quad \otimes A_r(\boldsymbol{x})[T^{-1}(\boldsymbol{\tau}) - S(\boldsymbol{x})]^{-1}) \frac{\partial \mathrm{vec}(T^{-1}(\boldsymbol{\tau}) - S(\boldsymbol{x}))}{\partial \boldsymbol{x}^T} \\
&\quad + (I_{N_t} \otimes A_r(\boldsymbol{x})[T^{-1}(\boldsymbol{\tau}) - S(\boldsymbol{x})]^{-1}) \frac{\partial \mathrm{vec}({A_t}^T(\boldsymbol{x}))}{\partial \boldsymbol{x}^T} \\
&= (A_t(\boldsymbol{x})[T^{-1}(\boldsymbol{\tau}) - S(\boldsymbol{x})]^{-1} \otimes I_{N_r})([I_M \otimes \mathbf{1}_n^T] \odot B_r(\boldsymbol{x})) \\
&\quad - (A_t(\boldsymbol{x})[T^{-1}(\boldsymbol{\tau}) - S(\boldsymbol{x})]^{-1} \\
&\quad \otimes A_r(\boldsymbol{x})[T^{-1}(\boldsymbol{\tau}) - S(\boldsymbol{x})]^{-1}) \frac{\partial \mathrm{vec}(S(\boldsymbol{x}))}{\partial \boldsymbol{x}^T} \\
&\quad + \big(I_{N_t} \otimes A_r(\boldsymbol{x})[T^{-1}(\boldsymbol{\tau}) - S(\boldsymbol{x})]^{-1}\big) U_{N_t,M} \frac{\partial \mathrm{vec}(A_t(\boldsymbol{x}))}{\partial \boldsymbol{x}^T} \\
&= A_t(\boldsymbol{x})[T^{-1}(\boldsymbol{\tau}) - S(\boldsymbol{x})]^{-1}(I_M \otimes \mathbf{1}_n^T) \odot B_r(\boldsymbol{x}) \\
&\quad - (A_t(\boldsymbol{x})[T^{-1}(\boldsymbol{\tau}) - S(\boldsymbol{x})]^{-1} \\
&\quad \otimes A_r(\boldsymbol{x})[T^{-1}(\boldsymbol{\tau}) - S(\boldsymbol{x})]^{-1}) \frac{\partial \mathrm{vec}(S(\boldsymbol{x}))}{\partial \boldsymbol{x}^T} \\
&\quad + (I_{N_t} \otimes A_r(\boldsymbol{x})[T^{-1}(\boldsymbol{\tau}) - S(\boldsymbol{x})]^{-1}) \\
&\quad \otimes U_{N_t,M}([I_M \otimes \mathbf{1}_n^T] \odot B_t(\boldsymbol{x})) \\
&= A_t(\boldsymbol{x})[T^{-1}(\boldsymbol{\tau}) - S(\boldsymbol{x})]^{-1}(I_M \otimes \mathbf{1}_n^T) \odot B_r(\boldsymbol{x}) \\
&\quad - (A_t(\boldsymbol{x})[T^{-1}(\boldsymbol{\tau}) - S(\boldsymbol{x})]^{-1} \\
&\quad \otimes A_r(\boldsymbol{x})[T^{-1}(\boldsymbol{\tau}) - S(\boldsymbol{x})]^{-1}) \frac{\partial \mathrm{vec}(S(\boldsymbol{x}))}{\partial \boldsymbol{x}^T} \\
&\quad + B_t(\boldsymbol{x}) \odot A_r(\boldsymbol{x})[T^{-1}(\boldsymbol{\tau}) - S(\boldsymbol{x})]^{-1}(I_M \otimes \mathbf{1}_n^T) \\
&= \big[A_t(\boldsymbol{x})[T^{-1}(\boldsymbol{\tau}) - S(\boldsymbol{x})]^{-1} \otimes \mathbf{1}_n^T\big] \odot B_r(\boldsymbol{x}) \\
&\quad - (A_t(\boldsymbol{x})[T^{-1}(\boldsymbol{\tau}) - S(\boldsymbol{x})]^{-1} \\
&\quad \otimes A_r(\boldsymbol{x})[T^{-1}(\boldsymbol{\tau}) - S(\boldsymbol{x})]^{-1}) \frac{\partial \mathrm{vec}(S(\boldsymbol{x}))}{\partial \boldsymbol{x}^T} \\
&\quad + B_t(\boldsymbol{x}) \odot \big[A_r(\boldsymbol{x})[T^{-1}(\boldsymbol{\tau}) - S(\boldsymbol{x})]^{-1} \otimes \mathbf{1}_n^T\big] \\
&= \big(A_t(\boldsymbol{x})[T^{-1}(\boldsymbol{\tau}) - S(\boldsymbol{x})]^{-1} \otimes \mathbf{1}_n^T\big) \odot B_r(\boldsymbol{x}) \\
&\quad - (A_t(\boldsymbol{x})[T^{-1}(\boldsymbol{\tau}) - S(\boldsymbol{x})]^{-1} \\
&\quad \otimes A_r(\boldsymbol{x})[T^{-1}(\boldsymbol{\tau}) - S(\boldsymbol{x})]^{-1})C(\boldsymbol{x}) \\
&\quad + B_t(\boldsymbol{x}) \odot (A_r(\boldsymbol{x})[T^{-1}(\boldsymbol{\tau}) - S(\boldsymbol{x})]^{-1} \otimes \mathbf{1}_n^T)
\end{aligned}
$$

where in the third equality, we used the identity [40]

$$
\begin{aligned}
&\frac{\partial \mathrm{vec}(UY^{-1}VZ^{-1}W)}{\partial \boldsymbol{x}^T} \\
&\quad = (W^T Z^{T-1} V^T Y^{T-1} \otimes I_q) \frac{\partial \mathrm{vec}(U)}{\partial \boldsymbol{x}^T} \\
&\qquad - (W^T Z^{T-1} V^T Y^{T-1} \otimes UY^{-1}) \frac{\partial \mathrm{vec}(Y)}{\partial \boldsymbol{x}^T} \\
&\qquad + (W^T Z^{T-1} \otimes UY^{-1}) \frac{\partial \mathrm{vec}(V)}{\partial \boldsymbol{x}^T} \\
&\qquad - (W^T Z^{T-1} \otimes UY^{-1}VZ^{-1}) \frac{\partial \mathrm{vec}(Z)}{\partial \boldsymbol{x}^T} \\
&\qquad + (I_r \otimes UY^{-1}VZ^{-1}) \frac{\partial \mathrm{vec}(W)}{\partial \boldsymbol{x}^T}.
\end{aligned}
$$

In the fourth equality, we used the identity $\partial \mathrm{vec}(A_r(\boldsymbol{x}))/\partial \boldsymbol{x}^T = [I_M \otimes \mathbf{1}_n^T] \odot B_r(\boldsymbol{x})$, which is easily verified. The commutation matrix $U_{m,n}$ [40], [50] in the fourth equality is the zero-one matrix such that $U_{m,n}\mathrm{vec}(A) = \mathrm{vec}(A^T)$ for any $A$ $(m \times n)$. In the fifth equality, we used the identity $(A \otimes B)(F \odot G) = (AF \odot BG)$ [42], and $\partial \mathrm{vec}(A_t(\boldsymbol{x}))/\partial \boldsymbol{x}^T = [I_M \otimes \mathbf{1}_n^T] \odot B_t(\boldsymbol{x})$. The sixth equality follows by Theorem 1, and in the seventh equality, we used $A(I \otimes \mathbf{1}_n^T) = A \otimes \mathbf{1}_n^T$. In the eighth equality

$$
\begin{aligned}
C(\boldsymbol{x}) &= [\boldsymbol{c}^T(\boldsymbol{x}_1), \boldsymbol{c}^T(\boldsymbol{x}_2) \cdots \boldsymbol{c}^T(\boldsymbol{x}_M)]^T \\
\boldsymbol{c}(\boldsymbol{x}_m) &= \partial \boldsymbol{g}(\boldsymbol{x}_m)/\partial \boldsymbol{x}^T, m = 1, 2, \ldots, M, \\
\boldsymbol{g}(\boldsymbol{x}_m) &= [G(\boldsymbol{x}_1, \boldsymbol{x}_m), G(\boldsymbol{x}_2, \boldsymbol{x}_m), \ldots, G(\boldsymbol{x}_M, \boldsymbol{x}_m)]^T
\end{aligned} \tag{A9}
$$

in which $G(\boldsymbol{x}_m, \boldsymbol{x}_m) \triangleq 0, m = 1, 2, \ldots, M$. □

*Theorem 1:* $(A \otimes B)U_{n,q}(C \odot D) = (AD \odot BC)$, where "$\otimes$" denotes the Kronecker product, "$\odot$" denotes the Khatri–Rao product, and $A$ $(m \times n)$, $B$ $(p \times q)$, $C$ $(q \times s)$, $D$ $(n \times s)$, $U_{n,q}$ is the commutation matrix.

*Proof:*

$$
\begin{aligned}
(A \otimes B)U_{n,q}(C \odot D) &= U_{m,p}U_{p,m}(A \otimes B)U_{n,q}(C \odot D) \\
&= U_{m,p}(B \otimes A)(C \odot D) \\
&= U_{m,p}(BC \odot AD) \\
&= AD \odot BC
\end{aligned} \tag{A10}
$$

where in the first equality, we used the $U_{m,p} = U_{p,m}^{-1}$ [42], the second $U_{p,m}(A \otimes B)U_{n,q} = (B \otimes A)$ [42], and the third $(B \otimes A)(C \odot D) = (BC \odot AD)$ follows from (T3.12) in [42]. The last equality is by Lemma 1. □

*Lemma 1:* $U_{m,p}B \odot A = A \odot B$, where "$\odot$" denotes the Khatri–Rao product, $A$ $(m \times n)$, $B$ $(p \times n)$, $U_{m,p}$ is the commutation matrix.

$$\begin{aligned}\frac{\partial G(\boldsymbol{x}_m,\boldsymbol{\alpha}_k)}{\partial x_{m1}} &= \frac{e^{i2\pi R_{m,k}/\lambda}\frac{i2\pi}{\lambda}\frac{\partial R_{m,k}}{\partial x_{m1}}\sqrt{2\pi R_{m,k}/\lambda} - e^{i2\pi R_{m,k}/\lambda}\frac{1}{2\sqrt{2\pi R_{m,k}/\lambda}}\frac{2\pi}{\lambda}\frac{\partial R_{m,k}}{\partial x_{m1}}}{2\pi R_{m,k}/\lambda}\\ &= \frac{\frac{i2\pi}{\lambda}\sqrt{2\pi R_{m,k}/\lambda} - \frac{1}{2\sqrt{2\pi R_{m,k}/\lambda}}\frac{2\pi}{\lambda}}{2\pi R_{m,k}/\lambda}e^{i2\pi R_{m,k}/\lambda}\frac{x_{m1}-\alpha_{k1}}{R_{m,k}}\\ &= G(\boldsymbol{x}_m,\boldsymbol{\alpha}_k)\frac{\frac{i2\pi}{\lambda}R_{m,k}-\frac{1}{2}}{R_{m,k}^2}(x_{m1}-\alpha_{k1})\end{aligned}$$

*Proof:* Let $A = [\boldsymbol{a}_1, \boldsymbol{a}_2 \cdots \boldsymbol{a}_n]$ and $B = [\boldsymbol{b}_1, \boldsymbol{b}_2 \cdots \boldsymbol{b}_n]$. Then $A \odot B = [\boldsymbol{a}_1 \otimes \boldsymbol{b}_1, \boldsymbol{a}_2 \otimes \boldsymbol{b}_2 \cdots \boldsymbol{a}_n \otimes \boldsymbol{b}_n]$, and

$$\begin{aligned}U_{m,p}B\odot A &= U_{m,p}[\boldsymbol{b}_1\otimes\boldsymbol{a}_1, \boldsymbol{b}_2\otimes\boldsymbol{a}_2\cdots\boldsymbol{b}_n\otimes\boldsymbol{a}_n]\\ &= [U_{m,p}(\boldsymbol{b}_1\otimes\boldsymbol{a}_1), U_{m,p}(\boldsymbol{b}_2\otimes\boldsymbol{a}_2)\cdots U_{m,p}(\boldsymbol{b}_n\otimes\boldsymbol{a}_n)]\\ &= [\boldsymbol{a}_1\otimes\boldsymbol{b}_1, \boldsymbol{a}_2\otimes\boldsymbol{b}_2\cdots\boldsymbol{a}_n\otimes\boldsymbol{b}_n]\\ &= A\odot B\end{aligned}$$

where the second equality comes from $U_{m,p}(\boldsymbol{b}\otimes\boldsymbol{a}) = U_{m,p}\mathrm{vec}(\boldsymbol{a}\boldsymbol{b}^T) = \mathrm{vec}(\boldsymbol{b}\boldsymbol{a}^T) = \boldsymbol{a}\otimes\boldsymbol{b}$, here $\boldsymbol{a}$ and $\boldsymbol{b}$ are vectors of dimension $m$ and $p$, respectively. □

## APPENDIX B

We use the 2-D Green's function in homogeneous medium as

$$G(\boldsymbol{x}_m,\boldsymbol{\alpha}_k) = \frac{e^{i2\pi R_{m,k}/\lambda}}{\sqrt{2\pi R_{m,k}/\lambda}} \tag{B1}$$

for $m = 1,2,\ldots,M$ and $k = 1,2,\ldots,N_t$, where $R_{m,k} = |\boldsymbol{x}_m - \boldsymbol{\alpha}_k| = \sqrt{(x_{m1}-\alpha_{k1})^2 + (x_{m2}-\alpha_{k2})^2}$ and the equation shown at the top of the page hold. where in the second equality we use $\partial R_{m,k}/\partial x_{m1} = (x_{m1}-\alpha_{k1})/R_{m,k}$. We can also find the following derivatives:

$$\frac{\partial G(\boldsymbol{x}_m,\boldsymbol{\alpha}_k)}{\partial x_{m2}} = G(\boldsymbol{x}_m,\boldsymbol{\alpha}_k)\frac{\frac{i2\pi}{\lambda}R_{m,k}-\frac{1}{2}}{R_{m,k}^2}(x_{m2}-\alpha_{k2}).$$

Then

$$\frac{\partial G(\boldsymbol{x}_m,\boldsymbol{\alpha}_k)}{\partial \boldsymbol{x}_m} = G(\boldsymbol{x}_m,\boldsymbol{\alpha}_k)\frac{\frac{i2\pi}{\lambda}|\boldsymbol{x}_m-\boldsymbol{\alpha}_k|-\frac{1}{2}}{|\boldsymbol{x}_m-\boldsymbol{\alpha}_k|^2}(\boldsymbol{x}_m-\boldsymbol{\alpha}_k)$$

and

$$\frac{\partial \boldsymbol{g}_t(\boldsymbol{x}_m)}{\partial \boldsymbol{x}_m^T} = \left[\frac{\partial G(\boldsymbol{x}_m,\boldsymbol{\alpha}_1)}{\partial \boldsymbol{x}_m}\cdots\frac{\partial G(\boldsymbol{x}_m,\boldsymbol{\alpha}_{N_t})}{\partial \boldsymbol{x}_m}\right]^T. \tag{B2}$$

Analogously

$$\frac{\partial G(\boldsymbol{\beta}_j,\boldsymbol{x}_m)}{\partial \boldsymbol{x}_m} = G(\boldsymbol{\beta}_j,\boldsymbol{x}_m)\frac{\frac{i2\pi}{\lambda}|\boldsymbol{x}_m-\boldsymbol{\beta}_j|-\frac{1}{2}}{|\boldsymbol{x}_m-\boldsymbol{\beta}_j|^2}(\boldsymbol{x}_m-\boldsymbol{\beta}_j),$$

and

$$\frac{\partial \boldsymbol{g}_r(\boldsymbol{x}_m)}{\partial \boldsymbol{x}_m^T} = \left[\frac{\partial G(\boldsymbol{\beta}_1,\boldsymbol{x}_m)}{\partial \boldsymbol{x}_m}\cdots\frac{\partial G(\boldsymbol{\beta}_{N_r},\boldsymbol{x}_m)}{\partial \boldsymbol{x}_m}\right]^T. \tag{B3}$$

## REFERENCES


[1] M. Fink, "Time-reversed acoustics," *Scientif. Amer.*, vol. 281, pp. 91–97, Nov. 1999.

[2] L. Borcea, G. Papanicolaou, and C. Tsogka, "Theory and applications of time reversal and interferometric imaging," *Inverse Problems*, vol. 19, pp. 5139–5164, 2003.

[3] L. Borcea, C. Tsogka, G. Papanicolaou, and J. Berryman, "Imaging and time reversal in random media," *Inverse Problems*, vol. 18, pp. 1247–1279, 2002.

[4] M. Born and E. Wolf, *Principles of Optics*. New York: Academic Press, 1970.

[5] M. Fink, D. Cassereau, A. Derode, C. Prada, P. Roux, M. Tanter, J. L. Thomas, and F. Wu, "Time-reversed acoustics," *Rep. Progr. Phys.*, vol. 63, pp. 1933–1995, 2000.

[6] M. Fink and C. Prada, "Acoustic time-reversal mirrors, topical review," *Inverse Problems*, vol. 17, pp. R1–R38, 2001.

[7] A. Derode, A. Tourin, and M. Fink, "Random multiple scattering of ultrasound. I. Coherent and ballistic waves," *Phys. Rev. E*, vol. 64, 2001, 036605.

[8] A. Derode, A. Tourin, and M. Fink, "Random multiple scattering of ultrasound. II. Is time reversal a self-averaging process?," *Phys. Rev. E*, vol. 64, 2001, 036606.

[9] H. Krim and M. Viberg, "Two decades of array signal processing research, the parametric approach," *IEEE Signal Process. Mag.*, vol. 13, no. 4, pp. 67–94, Jul. 1996.

[10] B. D. Van Veen and K. M. Buckley, "Beamforming: A versatile approach to spatial filtering," *IEEE ASSP Mag.*, vol. 5, no. 2, pp. 4–24, Apr. 1988.

[11] H. L. Van Trees, *Detection, Estimation, and Linear Modulation Theory. —Pt. 3. Radar-sonar Signal Processing and Gaussian Signals in Noise. —Pt. 4. Optimum Array Processing*. New York: Wiley, 2001.

[12] S. M. Kay, *Fundamentals of Statistical Signal Processing: Estimation Theory*. Englewood Cliffs, NJ: Prentice-Hall, 1993.

[13] P. Stoica and R. L. Moses, *Introduction to Spectral Analysis*. Upper Saddle River, NJ: Prentice-Hall, 1997.

[14] S. S. Haykin, *Detection and Estimation: Applications to Radar*. Stroudsburg, PA: Dowden, Hutchinson & Ross, 1976.

[15] H. V. Poor, *An Introduction to Signal Detection and Estimation*, 2nd ed. New York: Springer-Verlag, 1994.

[16] L. L. Scharf, *Statistical Signal Processing: Detection, Estimation and time Series Analysis*. Reading, MA: Addison-Wesley, 1991.

[17] A. Derode, P. Roux, and M. Fink, "Robust acoustic time reversal with high-order multiple scattering," *Phys. Rev. Lett.*, vol. 75, no. 23, pp. 4206–4210, 1995.

[18] A. Derode, P. Roux, and M. Fink, "Acoustic time-reversal through high-order multiple scattering," in *Proc. IEEE Ultrasonic Symp.*, 1995, pp. 1091–1094.

[19] A. Derode, A. Tourin, and M. Fink, "Time reversal versus phase conjugation in a multiple scattering environment," *Ultrasonics Int.*, vol. 40, no. 1, pp. 275–280, May 2002.

[20] A. Derode, A. Tourin, and M. Fink, "Multiple scattering and time-reversal acoustics," presented at the 17th Int. Congr. Acoust., Rome, Italy, 2001.

[21] A. Derode, A. Tourin, and M. Fink, "Optimisation of time-reversal focusing in a multiple scattering environment," presented at the 141st ASA Meeting, J. Acoust. Soc. Amer., Chicago, IL, 2001.

[22] A. Derode, A. Tourin, J. Rosny, M. Tanter, S. Yon, and M. Fink, "Taking advantage of multiple scattering to communication with time-reversal antennas," *Phys. Rev. Lett.*, vol. 90, no. 1, 2003, 014301.

[23] F. K. Gruber, E. A. Marengo, and A. J. Devaney, "Time-reversal imaging with multiple signal classification considering multiple scattering between the targets," *J. Acoust. Soc. Amer.*, vol. 115, pp. 3042–3047, Jun. 2004.
[24] A. J. Devaney, E. A. Marengo, and F. K. Gruber, "Time-reversal based imaging and inverse scattering of multiple scattering point targets," *J. Acoust. Soc. Amer.*, vol. 118, no. 5, pp. 3129–3138, Nov. 2005.
[25] G. Shi and A. Nehorai, "Maximum likelihood estimation of point scatterers for computational time-reversal imaging," presented at the 13th Annu. Workshop Adapt. Sensor Array Process., Lexington, MA, 2005.
[26] G. Shi and A. Nehorai, "Maximum likelihood estimation of point scatterers for computational time-reversal imaging," *Commun. Inf. Syst.*, vol. 5, no. 2, pp. 227–256, 2005.
[27] R. Rangarajan and A. O. Hero III, "Analysis of a multistatic adaptive target illumination and detection approach (MATILDA) to time reversal imaging," presented at the IMA "Hot Topics" Workshop: Adapt. Sensing Multimode Data Inversion, Minneapolis, MN, 2004.
[28] R. Rangarajan, N. Patwari, and A. O. Hero III, "Analysis of a multistatic adaptive target illumination and detection approach (MATILDA) to time reversal imaging," , to be published.
[29] J. H. Taylor, *Scattering Theory*. New York: Wiley, 1972.
[30] L. L. Foldy, "The multiple scattering of waves," *Phys. Rev.*, vol. 67, pp. 107–119, 1945.
[31] M. Lax, "Multiple scattering of waves," *Rev. Mod. Phys.*, vol. 23, pp. 287–310, 1951.
[32] M. Lax, "Multiple scattering of waves. II. The effective field in dense systems," *Phys. Rev.*, vol. 85, pp. 621–629, 1952.
[33] R. G. Newton, *Scattering Theory of Waves and Particles*. New York: McGraw-Hill, 1966.
[34] A. J. Devaney, "Super-resolution processing of multi-static data using time reversal and MUSIC," *J. Acoust. Soc. Amer.* [Online]. Available: http://www.ece.neu.edu/faculty/devaney, to be published
[35] A. J. Devaney, "Time reversal imaging of obscured targets from multistatic data," *IEEE Trans. Antennas Propag.*, vol. 53, no. 5, pp. 1600–1610, May 2005.
[36] C. Tai, *Dyadic Green Functions in Electromagnetic Theory*. Piscataway, NJ: IEEE Press, 1994.
[37] G. W. Stewart and J. Sun, *Matrix Perturbation Theory*. Boston, MA: Academic Press, 1990.
[38] P. M. Morse and H. Feshbach, *Methods of Theoretical Physics*. New York: McGraw-Hill, 1953.
[39] P. Stoica and A. Nehorai, "MUSIC, maximum likelihood and Cramér–Rao bound," *IEEE Trans. Acoust., Speech, Signal Process.*, vol. ASSP-37, no. 5, pp. 720–741, May 1989.
[40] H. Lütkepohl, *Handbook of Matrices*. New York: Wiley, 1996.
[41] B. Hochwald and A. Nehorai, "Concentrated Cramér–Rao bound expressions," *IEEE Trans. Inf. Theory*, vol. 40, no. 2, pp. 363–371, Mar. 1994.
[42] J. W. Brewer, "Kronecker products and matrix calculus in system theory," *IEEE Trans. Circuits Syst.*, vol. CAS-25, no. 9, pp. 772–781, Sep. 1978.
[43] P. Sheng, *Introduction to Wave Scattering, Localization, and Mesoscopic Phenomena*. San Diego, CA: Academic Press, 1995.
[44] G. Shi and A. Nehorai, "Macrocell multiple-input multiple-output system analysis," *IEEE Trans. Wireless Commun.*, vol. 5, no. 5, pp. 1076–1085, May 2006.
[45] J. R. Magnus and H. Neudecker, *Matrix Differential Calculus with Applications in Statistics and Econometrics*. New York: Wiley, 1999.
[46] D. H. Brandwood, "A complex gradient operator and its application in adaptive array theory," *Inst. Elect. Eng. Proc.*, vol. 130, no. 1, pp. 11–16, Feb. 1983.
[47] L. Schwartz, *Cours d'Analyse*. Paris, France: Hermann, 1967, vol. II.
[48] K. B. Petersen and M. S. Pedersen, "The Matrix Cookbook," 2006 [Online]. Available: http://2302.dk/uni/matrixcookbook.html
[49] H. Lev-Ari, "Efficient solution of linear matrix equations with application to multistatic antenna array processing," *Commun. Inf. Syst.*, vol. 5, no. 1, pp. 123–130, 2005.
[50] D. A. Turkington, *Matrix Calculus and Zero-one Matrices*. Cambridge, U.K.: Cambridge Univ. Press, 2002.

**Gang Shi** (S'02) received the B.E. degree in automatic control engineering and the M.E. degree in pattern recognition and intelligence system from the Xi'an Jiaotong University, Xi'an, China, in 1996 and 1999, respectively, and the D.Sc. degree in electrical engineering from Washington University in St. Louis, MO, in 2006.

He is currently a Postdoctoral Researcher at Biostatistics Division, Washington University School of Medicine. From 1999 to 2000, he worked as a Teaching Associate at the Xi'an Jiaotong University.

**Arye Nehorai** (S'80–M'83–SM'90–F'94) received the B.Sc. and M.Sc. degrees in electrical engineering from The Technion, Haifa, Israel, and the Ph.D. degree in electrical engineering from Stanford University, Stanford, CA.

From 1985 to 1995, he was a faculty member with the Department of Electrical Engineering, Yale University, New Haven, CT. In 1995, he joined the Department of Electrical Engineering and Computer Science, The University of Illinois at Chicago (UIC), as a Full Professor. From 2000 to 2001, he was Chair of the department's Electrical and Computer Engineering (ECE) Division, which then became a new department. In 2001, he was named University Scholar of the University of Illinois. In 2006, he became Chairman of the Department of Electrical and Systems Engineering, Washington University in St. Louis (WUSTL). He is the inaugural holder of the Eugene and Martha Lohman Professorship and the Director of the Center for Sensor Signal and Information Processing (CSSIP) at WUSTL since 2006.

Dr. Nehorai was co-recipient of the IEEE SPS 1989 Senior Award for Best Paper with P. Stoica, co-author of the 2003 Young Author Best Paper Award, and co-recipient of the 2004 Magazine Paper Award with A. Dogandzic. He was elected Distinguished Lecturer of the IEEE SPS for the term 2004 to 2005. He is the Principal Investigator of the New Multidisciplinary University Research Initiative (MURI) Project entitled Adaptive Waveform Diversity for Full Spectral Dominance. He has been a Fellow of the Royal Statistical Society since 1996. He was Editor-in-Chief of the IEEE TRANSACTIONS ON SIGNAL PROCESSING during the years 2000 to 2002. In the years 2003 to 2005, he was Vice President (Publications) of the IEEE Signal Processing Society, Chair of the Publications Board, member of the Board of Governors, and member of the Executive Committee of this Society. From 2003 to 2006, he was the founding editor of the special columns on Leadership Reflections in the *IEEE Signal Processing Magazine*.